Journal of Geotechnical and Geoenvironmental Engineering, Vol. 139, No. 1, pp. 59-72, 2013

Effect of uniformity coefficient on $G/G_{\max}$ and damping ratio of uniform to well graded quartz sands

T. Wichtmann[i)], Th. Triantafyllidis[ii)]

Abstract: The modulus degradation curves $G(\gamma)/G_{\max}$ and the damping ratio $D(\gamma)$ of 27 clean quartz sands with specially mixed grain size distribution curves were measured in approximately 280 resonant column tests. For each material, tests with different pressures and densities were performed. Based on the test data it is demonstrated that the shear modulus degradation is larger for higher values of the uniformity coefficient, $C_u = d_{60}/d_{10}$, while it is rather independent of the mean grain size, d_{50}. The observed C_u-dependence of the curves $G(\gamma)/G_{\max}$ is not adequately described by common empirical equations, because theses equations were developed based on tests on uniform granular materials. In order to consider the influence of the uniformity coefficient, the paper proposes correlations of the parameters of the common empirical equations with C_u. Good agreement between the prediction of the extended empirical equations and experimental data collected from the literature is demonstrated. Furthermore, the test data reveal that the curves of damping ratio, $D(\gamma)$, and the threshold shear strain amplitude indicating the onset of residual deformation accumulation, γ_{tv}, are rather independent of d_{50} and C_u. The threshold shear strain amplitude at the onset of modulus degradation, γ_{tl}, slightly decreases with increasing values of d_{50} and C_u.

CE Database subject headings: Shear modulus; Damping ratio; Quartz sand; Grain size distribution curve; Uniformity coefficient; Resonant column tests;

1 Introduction

The secant shear modulus, G, and the damping ratio, D, are key design parameters for soils subjected to dynamic loading. It is well known that both quantities are strongly strain-dependent. If a certain threshold value of the shear strain amplitude, γ, is surpassed, the shear modulus, G, decreases with γ while the damping ratio, D, increases. Contrary to the small-strain shear modulus, $G_{\max} = G(\gamma < 10^{-6})$, which can be determined from shear wave velocity measurements, the modulus degradation curves, $G(\gamma)/G_{\max}$, and the damping ratio, $D(\gamma)$, cannot be easily quantified in-situ. Therefore, if laboratory test data are not available, the modulus degradation and the damping ratio are often estimated by means of empirical equations or chosen based on typical ranges provided in the literature (see the summary in Section 2).

The common empirical equations for $G(\gamma)/G_{\max}$ and $D(\gamma)$ were developed based on tests on granular materials with uniform grain size distribution curves. It has not been proven experimentally yet that these equations are also applicable to well-graded granular materials. Wichtmann & Triantafyllidis [35, 36] have demonstrated that the common empirical equations for the small-strain shear modulus ,$G_{\max}$, e.g. the formula proposed by Hardin and Black [4], do not adequately describe the C_u-dependence of $G_{\max}$ observed in laboratory tests. In those tests, for constant values of void ratio and mean pressure, the small-strain shear modulus, $G_{\max}$, and the P-wave velocity, v_P, were found independent of mean grain size, d_{50}, but strongly decreasing with increasing uniformity coefficient, $C_u = d_{60}/d_{10}$. In order to consider this influence, correlations of the parameters of several empirical equations for $G_{\max}$ and v_P with C_u have been proposed by Wichtmann & Triantafyllidis [35, 36].

Based on the data from approximately 280 resonant column tests performed on 27 clean quartz sands, the present paper examines the influence of the grain size distribution curve on modulus degradation, $G(\gamma)/G_{\max}$, on damping ratio, $D(\gamma)$ and on the threshold shear strain amplitudes, γ_{tl} and γ_{tv}, indicating the onset of modulus degradation or the onset of residual deformation accumulation, respectively. The need for an extension of the common empirical equations describing modulus degradation considering the influence of C_u is demonstrated.

2 Empirical equations for $G(\gamma)/G_{\max}$ and $D(\gamma)$

It is well known that the modulus degradation and the damping ratio are pressure-dependent. For certain shear strain amplitude, the ratio $G/G_{\max}$ increases with increasing pressure while the damping ratio, D, decreases (Hardin & Drnevich [6], Kokusho [11], Seed et al. [25]). In contrast, the curves $G(\gamma)/G_{\max}$ and $D(\gamma)$ are rather independent of soil density (e.g. Kokusho [11]).

Several empirical formulas have been proposed in the literature. Those used in this paper are presented in the following. Hardin & Drnevich [5] describe the curves $G(\gamma)/G_{\max}$ by:

$$\frac{G}{G_{\max}} = \frac{1}{1+\frac{\gamma}{\gamma_r}} \tag{1}$$

or by the more flexible function

$$\frac{G}{G_{\max}} = \frac{1}{1+\frac{\gamma}{\gamma_r}\ \left[1+a\ \exp\left(-b\ \frac{\gamma}{\gamma_r}\right)\right]} \tag{2}$$

with two curve-fitting parameters a and b and with the reference shear strain defined as

$$\gamma_r = \frac{\tau_{\max}}{G_{\max}} \tag{3}$$

[i)] Research Assistant, Institute of Soil Mechanics and Rock Mechanics, Karlsruhe Institute of Technology (KIT), Germany (corresponding author). Email: torsten.wichtmann@ibf.uka.de

[ii)] Professor and Director of the Institute of Soil Mechanics and Rock Mechanics, Karlsruhe Institute of Technology (KIT), Germany

where τ_{max} is the shear strength. Hardin & Kalinski [7] demonstrated that a normalization of γ with a simplified factor $\sqrt{p/p_{atm}}$ instead of γ_r (p = effective mean pressure, p_{atm} = 100 kPa) is also suitable to purify the modulus degradation curves from the influence of pressure. In that case no information about τ_{max} is necessary. According to Hardin & Kalinski [7], setting $b = 1$ in Eq. (2) is sufficient in order to describe the modulus degradation curves.

A modification of Eq. (1) was proposed by Stokoe et al. [28]:

$$\frac{G}{G_{max}} = \frac{1}{1+(\gamma/\gamma_r)^{\alpha}} \quad (4)$$

with the curvature parameter α. Unlike Eq. (3), the reference shear strain used in Eq. (4) is defined as $\gamma_r = \gamma(G/G_{max} = 0.5)$. The pressure-dependence of γ_r can be described by (Stokoe et al. [28]):

$$\gamma_r = \gamma_{r1}\,(p/p_{atm})^k \quad (5)$$

with the reference shear strain, γ_{r1}, at $p = p_{atm}$ = 100 kPa and with an exponent k.

Hardin & Drnevich [5] proposed the following formulas for the damping ratio, $D(\gamma)$:

$$\frac{D}{D_{max}} = \frac{\frac{\gamma}{\gamma_r}}{1+\frac{\gamma}{\gamma_r}} \quad \text{and} \quad (6)$$

$$\frac{D}{D_{max}} = \frac{\frac{\gamma}{\gamma_r}\left[1+a\,\exp\left(-b\,\frac{\gamma}{\gamma_r}\right)\right]}{1+\frac{\gamma}{\gamma_r}\left[1+a\,\exp\left(-b\,\frac{\gamma}{\gamma_r}\right)\right]} \quad (7)$$

Therein D_{max} is an asymptotic value of D at large strain amplitudes and a and b are curve-fitting parameters. Alternatively, damping ratio is often formulated as a function of G/G_{max} (e.g. Hardin & Drnevich [5], Tatsuoka et al. [30], Khouri [10]). Zhang et al. [40] described this relationship by

$$D - D_{min} = c_1\,(G/G_{max})^2 + c_2\,(G/G_{max}) - (c_1 + c_2) \quad (8)$$

with the minimum damping ratio, D_{min}, at very small shear strain amplitudes and with parameters c_1 = 0.106, c_2 = -0.316 for torsional shear test data and c_1 = 0.094, c_2 = -0.265 for resonant column (RC) test data. The equation proposed by Khouri [10] based on experimental data collected from the literature is retrieved from Eq. (8) with D_{min} = 0.013, c_1 = 0.195 and c_2 = -0.515.

The various empirical equations are inspected in the following sections, based on the data from the present test series.

3 Tested materials, test device and testing procedure

The natural quartz sand and gravel used for the present study was obtained from a sand pit near Dorsten, Germany. Its grain shape is sub-angular and the specific gravity is ϱ_s = 2.65 g/cm^3. First, the granular material was sieved into 25 gradations with grain sizes between 0.063 mm and 16 mm. Then, the grain size distribution curves shown in Fig. 1 were mixed from these gradations. They are linear in the semilogarithmic scale. The sands and gravels L1 to L8 (Fig. 1a) have a uniformity coefficient of C_u = 1.5 and different mean grain sizes in the range $0.1 \le d_{50} \le 6$ mm. These materials were used to study the influence of d_{50}. The materials

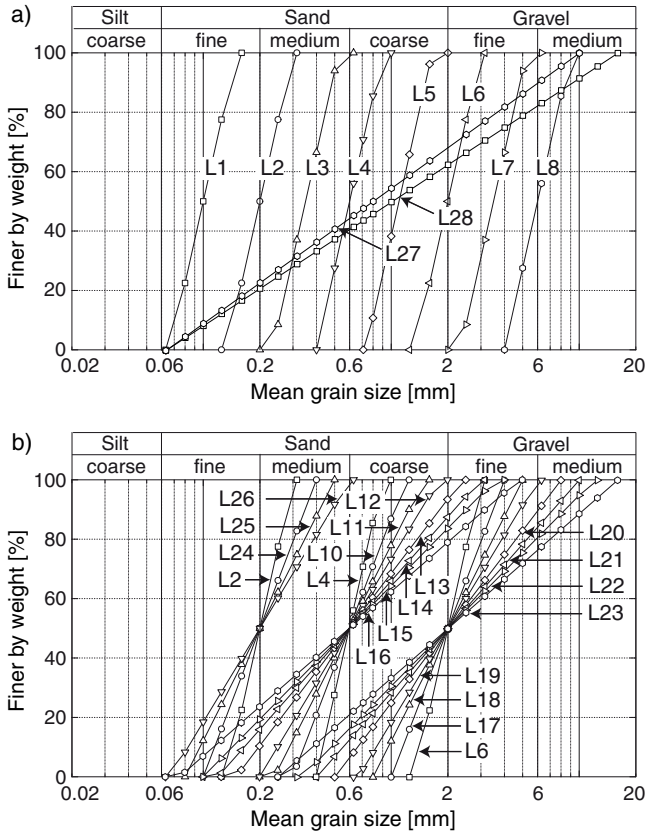

Fig. 1: *Tested grain size distribution curves (adapted from Wichtmann & Triantafyllidis [35])*

L24 to L26 (d_{50} = 0.2 mm, $2 \le C_u \le 3$), L10 to L16 (d_{50} = 0.6 mm, $2 \le C_u \le 8$) and L17 to L23 (d_{50} = 2 mm, $2 \le C_u \le 8$, Fig. 1b) were used to study the C_u-influence for different values of d_{50}. The two sand-gravel-mixtures L27 and L28 (Fig. 1a) have even higher uniformity coefficients (C_u = 12.6 and 15.9). The d_{50}- and C_u-values as well as the minimum and maximum void ratios of the tested materials are summarized in Table 1.

The resonant column (RC) device used for the present study (see a scheme and a foto given by Wichtmann & Triantafyllidis [35]) is a "free - free" type, meaning both the top and the base mass are freely rotatable. The cuboidal top mass is equipped with two electrodynamic exciters each accelerating a small mass. This acceleration and the resulting acceleration of the top mass are measured with accelerometers. From these signals the torsional moment, $M(t)$, and the angle of twist, $\theta(t)$, at the top of the sample can be calculated. The sample is enclosed in a pressure cell that can sustain cell air pressures, σ_3, up to 800 kPa. The state of stress is almost isotropic. A small stress anisotropy results from the weight of the top mass ($m \approx 9$ kg), such that the vertical stress, σ_1, is slightly higher than the lateral one, σ_3. However, for higher cell pressures this anisotropy is of secondary importance. Furthermore, test results of Yu & Richart [39] revealed that a stress anisotropy becomes significant only near failure.

A sinusoidal electrical signal is generated by a function generator, amplified and applied to the electrodynamic exciters. The frequency of excitation is varied until the resonant frequency, f_R, of the system composed of the two end masses and the specimen has been found. By definition, this is the

Mat.	d_{50} [mm]	C_u [-]	$e_{\min}$ [-]	$e_{\max}$ [-]	Range of tested D_{r0}	Mat.	d_{50} [mm]	C_u [-]	$e_{\min}$ [-]	$e_{\max}$ [-]	Range of tested D_{r0}	Mat.	d_{50} [mm]	C_u [-]	$e_{\min}$ [-]	$e_{\max}$ [-]	Range of tested D_{r0}
L1	0.1	1.5	0.634	1.127	0.46-0.78	L11	0.6	2.5	0.495	0.856	0.46-1.00	L20	2	4	0.439	0.728	0.65-1.00
L2	0.2	1.5	0.596	0.994	0.45-0.94	L12	0.6	3	0.474	0.829	0.45-0.93	L21	2	5	0.401	0.703	0.61-0.99
L3	0.35	1.5	0.591	0.931	0.42-0.98	L13	0.6	4	0.414	0.791	0.47-0.87	L22	2	6	0.401	0.553	0.39-1.04
L4	0.6	1.5	0.571	0.891	0.43-1.05	L14	0.6	5	0.394	0.749	0.46-0.84	L23	2	8	0.398	0.521	0.45-1.04
L5	1.1	1.5	0.580	0.879	0.46-1.02	L15	0.6	6	0.387	0.719	0.54-0.86	L24	0.2	2	0.559	0.958	0.52-0.93
L6	2	1.5	0.591	0.877	0.48-0.95	L16	0.6	8	0.356	0.673	0.51-0.87	L25	0.2	2.5	0.545	0.937	0.61-0.95
L7	3.5	1.5	0.626	0.817	0.49-0.99	L17	2	2	0.555	0.827	0.50-0.98	L26	0.2	3	0.540	0.920	0.64-0.93
L8	6	1.5	0.634	0.799	0.38-1.10	L18	2	2.5	0.513	0.810	0.54-0.99	L27	0.79	12.6	0.327	0.564	0.66-0.94
L10	0.6	2	0.541	0.864	0.43-1.02	L19	2	3	0.491	0.783	0.64-1.00	L28	1.0	15.9	0.300	0.460	0.54-0.96

Table 1: Parameters d_{50}, C_u, $e_{\min}$ and $e_{\max}$ (determined according to German standard code DIN 18126) of the tested grain size distribution curves, range of tested initial relative densities D_{r0}

case when $M(t)$ and $\theta(t)$ have a phase-shift of $\pi/2$ in time, t. The secant shear modulus

$$G = \left(\frac{2\pi\ h\ f_R}{a}\right)^2 \varrho \tag{9}$$

is calculated from the resonant frequency, the height, h, and the density, ϱ, of the specimen. The parameter a is obtained from:

$$a\ \tan(a) - \frac{J^2}{J_0\ J_L}\ \frac{\tan(a)}{a} = \frac{J}{J_0} + \frac{J}{J_L} \tag{10}$$

In Eq. (10), J, $J_0 = 1.176$ kg m^2, and $J_L = 0.0663$ kg m^2 are the polar mass moments of inertia of the specimen, the base mass and the top mass, respectively. The polar mass moment of inertia of the top mass has been calibrated by means of aluminium rods with different diameters and known stiffnesses.

Different shear strain amplitudes can be tested by varying the amplitude of the torsional excitation. All tested specimens had a full cross section and measured $d = 10$ cm in diameter and $h = 20$ cm in height. The variation of the shear strain amplitude with radius, r, and distance, x, from the base of the sample can be calculated from

$$\gamma(r,x) = -r\ \frac{\theta(x=h)}{\cos(a) - \frac{J_0}{J}\ a\ \sin(a)}\ \frac{a}{h} \left[\sin\left(\frac{ax}{h}\right) + \frac{J_0}{J}\ a\ \cos\left(\frac{ax}{h}\right)\right] \tag{11}$$

with the amplitude of the angle of twist $\theta(x = h)$ measured at the top of the sample. Evaluating Eq. (11) for typical a-values reveals only a slight variation of γ with x (about 2%). The variation with r is considered by calculating a mean value over the sample volume:

$$\bar{\gamma} = \frac{1}{V} \int_V \gamma(r,x)\ \mathrm{d}V \tag{12}$$

This mean value is simply denoted by γ in the following analysis of the test results. The shear strain amplitudes that can be tested in the device lie in the range $5 \times 10^{-7} \leq \gamma \leq 5 \times 10^{-4}$.

Measurements of the shear wave velocity by means of bender elements delivered very similar $G_{\max}$ values compared to tests performed with the RC device [37]. Preliminary tests on hollow cylinder samples (outer diameter $d_a = 10$ cm, inner diameter $d_i = 6$ cm, $h = 10$ cm), having a more uniform distribution of shear strains over the cross section, showed similar curves, $G(\gamma)$ and $D(\gamma)$, as full cylinder specimens. Therefore, the use of full cylinder specimens was regarded as sufficient for the present study. The comparison was undertaken for a medium coarse uniform sand. However, the conclusion is assumed valid also for more well-graded sands.

The settlement of the samples was measured with a non-contact displacement transducer placed approximately 1 mm above the center of the top mass, i.e., in a position where the torsional displacement is very small. This gap sensor measures against an aluminium target rigidly connected to the top mass.

All samples were prepared by air pluviation and tested in the air-dry condition. For each material, five to ten tests with different initial relative densities $D_{r0} = (e_{\max} - e_0)/(e_{\max} - e_{\min})$ were performed. The tested ranges of relative densities are given in Table 1. The mean pressure, p, was increased step-wise from $p = 50$ to 400 kPa in order to obtain the $G_{\max}$- and v_P-data documented by Wichtmann & Triantafyllidis [35,36]. The curves $G(\gamma)$ and $D(\gamma)$ were measured at $p = 400$ kPa. In three additional tests on medium dense specimens, the modulus degradation and the damping ratio were also measured at $p = 50$, 100 and 200 kPa.

The shear strength, $\tau_{\max}$, is necessary in order to calculate the reference shear strain, γ_r, from Eq. (3). For each material, the peak friction angle, φ_P, was determined from at least three monotonic triaxial tests on isotropically consolidated ($p_0 = 100$ kPa) samples prepared with different relative densities. The measured decrease of the peak-friction angle with increasing void ratio was described by an exponentially decreasing function, $\varphi_P(e_0)$, where e_0 is the initial void ratio of the sample before shearing.

4 Test results

4.1 Modulus degradation

4.1.1 Influence of d_{50} and C_u

For a constant value of the strain amplitude, the data from the present test series confirm the well-known increase of $G/G_{\max}$ with increasing mean pressure and the independence of density. This becomes obvious from Figure 2a-d where the modulus degradation curves for different pressures and densities are presented for four selected materials. The first three diagrams show the data for the three sands L4, L12 and L16, having a mean grain size of $d_{50} = 0.6$ mm and uniformity coefficients between $C_u = 1.5$ and 8. The fourth diagram contains data for the sand-gravel-mixture L28 ($C_u = 15.9$). The typical range of $G/G_{\max}$-values specified by

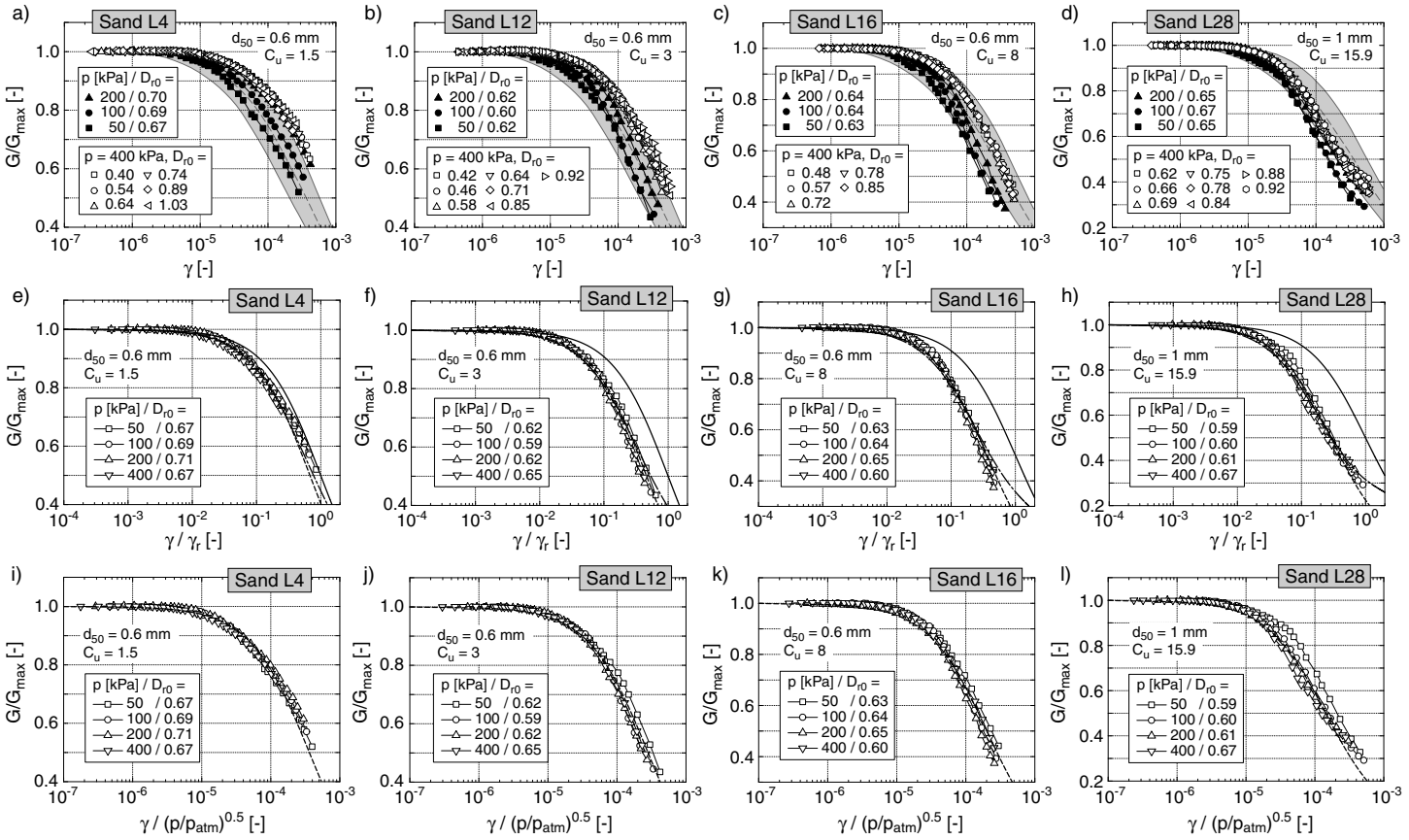

Fig. 2: *a-d) Modulus degradation curves $G(\gamma)/G_{\max}$ measured for different materials, pressures and densities (gray shading = range specified by Seed et al. [25]), e-h) $G/G_{\max}$ versus γ/γ_r (solid curves = Eq. (1), dot-dashed curves = Eq. (2) with $b = 1$, dashed curves = Eq. (14). i-l) $G/G_{\max}$ versus $\gamma/\sqrt{p/p_{atm}}$ (dashed curves = Eq. (2) with $b = 1$ and with $\sqrt{p/p_{atm}}$ instead of γ_r).*

Seed et al. [25] (based on Seed & Idriss [24]) is marked by the gray shading in Figure 2a-d. For poorly graded materials (e.g. L4), the curves $G(\gamma)/G_{\max}$ for $p = 50$ and 100 kPa fall into this range while the curves for $p = 200$ and 400 kPa lie slightly above. For intermediate uniformity coefficients ($3 \le C_u \le 5$, e.g. L12), the data for all tested pressures coincide well with the range specified by Seed et al. [25]. For well-graded granular materials ($C_u \ge 8$, e.g. L16, L28) the data for the lower pressures lie below the lower bound of the range of Seed et al. [25], in particular at higher shear strain amplitudes.

The influence of the mean grain size, d_{50}, on the modulus degradation curves is inspected in Figure 3a which compares the curves $G(\gamma)/G_{\max}$ measured for the sands and gravels L1 to L8, having the same uniformity coefficient $C_u = 1.5$ but different mean grain sizes in the range $0.1 \le d_{50} \le 6$ mm. All samples were medium dense and the mean pressure was 400 kPa in all tests. No clear tendency can be observed in Figure 3a. For a closer examination, the $G/G_{\max}$-data for certain values of the shear strain amplitude are plotted versus d_{50} in Figure 3b,c. The data are provided for $p = 100$ and 400 kPa. A small tendency for $G/G_{\max}$ to decrease with increasing d_{50} can be concluded from Figure 3b,c. However, this slight d_{50}-dependence can be neglected for practical purpose.

The influence of the uniformity coefficient, C_u, on the modulus degradation curves is examined in Figure 3d. It compares the $G(\gamma)/G_{\max}$ curves measured for the materials L6 and L17 to L23, having the same mean grain size d_{50} = 2 mm but different uniformity coefficients in the range $1.5 \le C_u \le 8$. The data are provided for a mean pressure p = 100 kPa. Obviously, the modulus degradation is larger for higher C_u-values. This becomes even clearer from Figure 3e,f where the $G/G_{\max}$-data for certain values of the shear strain amplitude are plotted versus C_u. For example, for a pressure $p = 100$ kPa and a shear strain amplitude $\gamma = 2 \cdot 10^{-4}$, the ratio $G/G_{\max}$ drops from about 0.7 for $C_u = 1.5$ to slightly above 0.4 for $C_u = 15.9$ (Figure 3e). The decrease of $G/G_{\max}$ with increasing C_u is similar for the three tested mean grain sizes d_{50} = 0.2, 0.6 and 2 mm (Figure 3e,f). Based on these test results it seems indispensable to consider the influence of the uniformity coefficient in empirical formulas describing modulus degradation.

4.1.2 Inspection of Hardin's equation (1)

The applicability of Eq. (1) has been inspected in Figure 2e-h, where the $G/G_{\max}$ data measured in the four tests with different pressures are plotted versus a normalized shear strain amplitude γ/γ_r. The data are provided for the four materials L4, L12, L16 and L28 but look similar for the other tested materials. The reference shear strain, γ_r, was calculated from Eq. (3), with the maximum shear modulus, $G_{\max}$, measured in the RC test. The shear strength was obtained from $\tau_{\max} = p \sin\varphi_P$ with the pressure, p, applied in the RC test and where φ_P is the peak friction angle. The peak friction angle was calculated from the relationship $\varphi_P(e_0)$ derived from the monotonic triaxial tests, with e_0 being the

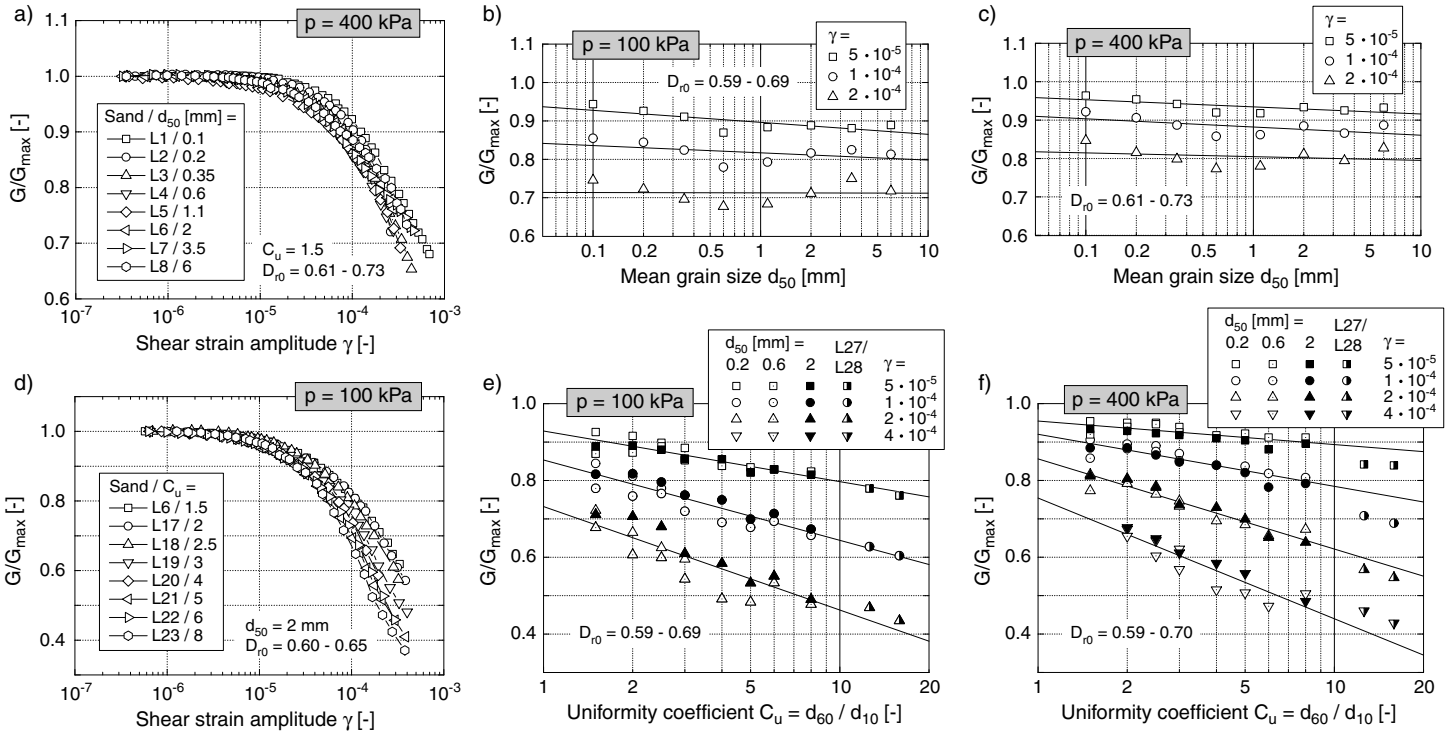

Fig. 3: *Dependence of modulus degradation on a)-c) mean grain size d_{50} and d)-f) uniformity coefficient C_u*

actual void ratio of the RC test sample at pressure p. As obvious from Figure 2e-h, the curves $G(\gamma/\gamma_r)/G_{\max}$ for different pressures fall together.

The prediction by Eq. (1) has been added as solid curves in Figure 2e-h. While Eq. (1) fits well for poorly graded sands (e.g. L4), it significantly underestimates the modulus degradation for well-graded granular materials (e.g. L16 and L28).

4.1.3 Extension of Hardin's equation (2)

Eq. (2) with $b = 1$ could be fitted well to the data of all tested materials (dot-dashed curves in Figure 2e-h). The 'a' parameter of Eq. (2) is plotted versus the uniformity coefficient in Figure 4a. The nearly linear increase of a with $\ln(C_u)$ can be approximated by (solid line in Figure 4a):

$$a = 1.070\ \ln(C_u) \tag{13}$$

4.1.4 Modification of Hardin's equation (1)

Based on the experimental results in this study, a simple modification of Eq. (1) was found suitable as well (dashed curves in Figure 2e-h):

$$\frac{G}{G_{\max}} = \frac{1}{1 + d\ \gamma/\gamma_r} \tag{14}$$

The curve-fitting parameter d of Eq. (14) is shown as a function of C_u in Figure 4b. The following correlation between d and C_u could be established (solid line in Figure 4b):

$$d = 1 + 0.847\ \ln(C_u) \tag{15}$$

4.1.5 Normalization with $\sqrt{p/p_{\mathbf{atm}}}$ instead of γ_r

The diagrams in Figure 2i-l demonstrate that the normalization of the shear strain amplitude with a factor $\sqrt{p/p_{\mathrm{atm}}}$ as proposed by Hardin & Kalinski [7] is also suitable. For each tested material, the data $G(\gamma/\sqrt{p/p_{\mathrm{atm}}})/G_{\max}$ for different pressures fall together into a narrow band which can be approximated by Eq. (2) with $b = 1$ and with $\sqrt{p/p_{\mathrm{atm}}}$ instead of γ_r (dashed curves in Figure 2i-l). The resulting 'a' parameter of Eq. (2) is plotted versus C_u in Figure 4c. The increase of a with C_u can be described by (solid line in Figure 4c):

$$a = 1093.7 + 1955.3\ \ln(C_u) \tag{16}$$

The curves obtained from a curve-fitting of Eq. (14) with $\sqrt{p/p_{\mathrm{atm}}}$ instead of γ_r are very similar to the dashed curves in Figure 2i-l. The correlation between the parameter d of Eq. (14) and the uniformity coefficient can be sufficiently well described by Eq. (16) with d instead of a.

4.1.6 Extension of Stokoe et al. [28] equations (4) and (5)

A curve-fitting of Eq. (4) to the $G(\gamma)/G_{\max}$-curves of all tested materials delivered the reference shear strain, $\gamma_r = \gamma(G/G_{\max} = 0.5)$, and the curvature parameter, α. The parameter α neither depends on density nor on pressure. The latter is in accordance with Zhang et al. [40]. Subsequently γ_r was plotted versus mean pressure p and Eq. (5) was fitted to these data, delivering the parameters γ_{r1} and k. In Figure 4d-f the parameters α, γ_{r1} and k obtained for the various materials are plotted as a function of the uniformity coefficient. The slight increase of α with increasing C_u (Figure 4d) can be neglected for practical purpose. It is recommended to use the mean value $\alpha = 1.03$. The parameter γ_{r1} strongly decreases with increasing C_u (Figure 4e) which can be described by (solid curve in Figure 4e):

$$\gamma_{r1} = 6.52 \cdot 10^{-4}\ \exp[-0.59 \ln(C_u)] \tag{17}$$

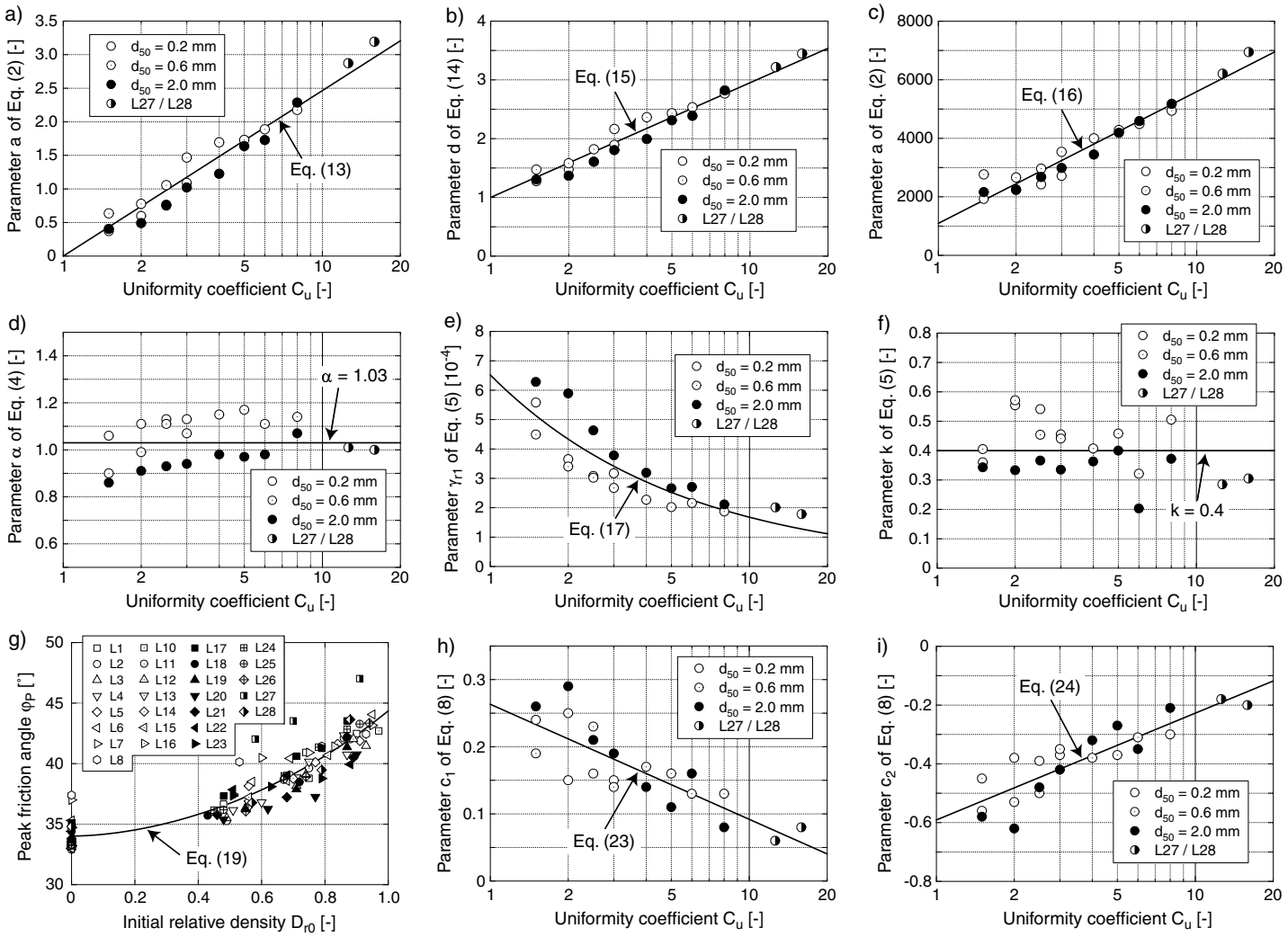

Fig. 4: *Correlation of the parameters of various empirical equations with the uniformity coefficient C_u: a) Parameter 'a' in Eq. (2), b) Parameter 'd' in Eq. (14), c) Parameter 'a' in Eq. (2) with $\sqrt{p/p_{atm}}$ instead of γ_r, d) Parameter α in Eq. (4), e,f) Parameters γ_{r1} and k in Eq. (5), g) Peak friction angle φ_P versus initial relative density D_{r0}, h),i) Parameters c_1 and c_2 in Eq. (8)*

The parameter k shows a significant scatter when plotted versus C_u (Figure 4f). For a practical application it is recommended to use the mean value $k = 0.4$ (solid line in Figure 4f). The error made by this assumption increases with increasing pressure. It has been inspected for the largest tested pressure $p = 400$ kPa and a shear strain amplitude $\gamma = 5 \cdot 10^{-4}$, using $\alpha = 1.03$ and γ_{r1} according to Eq. (17). The maximum or minimum k values ≈ 0.6 and ≈ 0.2 were obtained for sands with $C_u = 2$ or $C_u = 6$, respectively (see Figure 4f). For $C_u = 2$, the predicted $G/G_{\max}$ values are 0.67 for $k = 0.6$ and 0.60 for $k = 0.4$. For $C_u = 6$, the values are 0.37 for $k = 0.2$ and 0.44 for $k = 0.4$. These differences are considered small enough to justify the assumption of a constant $k = 0.4$.

4.1.7 Estimation of reference shear strain, γ_r

For an application of Eq. (2), one also needs an estimate of the reference shear strain, $\gamma_r = \tau_{\max}/G_{\max}$. The small-strain shear modulus can be obtained from the correlations proposed by Wichtmann and Triantafyllidis [35]. For cohesionless soils, the maximum shear stress, $\tau_{\max}$, can be calculated from:

$$\tau_{\max} = \sigma_v' \sqrt{\left(\frac{1+K_0}{2}\sin\varphi_P\right)^2 - \left(\frac{1-K_0}{2}\right)^2} \qquad (18)$$

with the vertical effective stress, σ_v', and the lateral stress coefficient, $K_0 = \sigma_h'/\sigma_v'$. Figure 4g collects the data of the peak friction angle, φ_P, as a function of initial relative density D_{r0} for all tested materials. The φ_P-values at $D_{r0} = 0$ were obtained from the inclination of a loosely pluviated cone of sand while all other φ_P-values were obtained from drained monotonic triaxial tests. No clear dependence of φ_P on the mean grain size, d_{50}, or on the uniformity coefficient, C_u, can be detected from the data in Figure 4g. The formula

$$\varphi_P = 34.0^\circ \exp(0.27\ {D_{r0}}^{1.8}) \qquad (19)$$

(solid curve in Figure 4g) can be used for an estimation of φ_P if no triaxial test data are available.

Alternatively, Eq. (5) can be applied to estimate γ_r used in Eq. (2). Based on the data of the present study, the parameter γ_{r1} of Eq. (5) is almost independent of C_u. The relationship between γ_{r1} and initial relative density can be

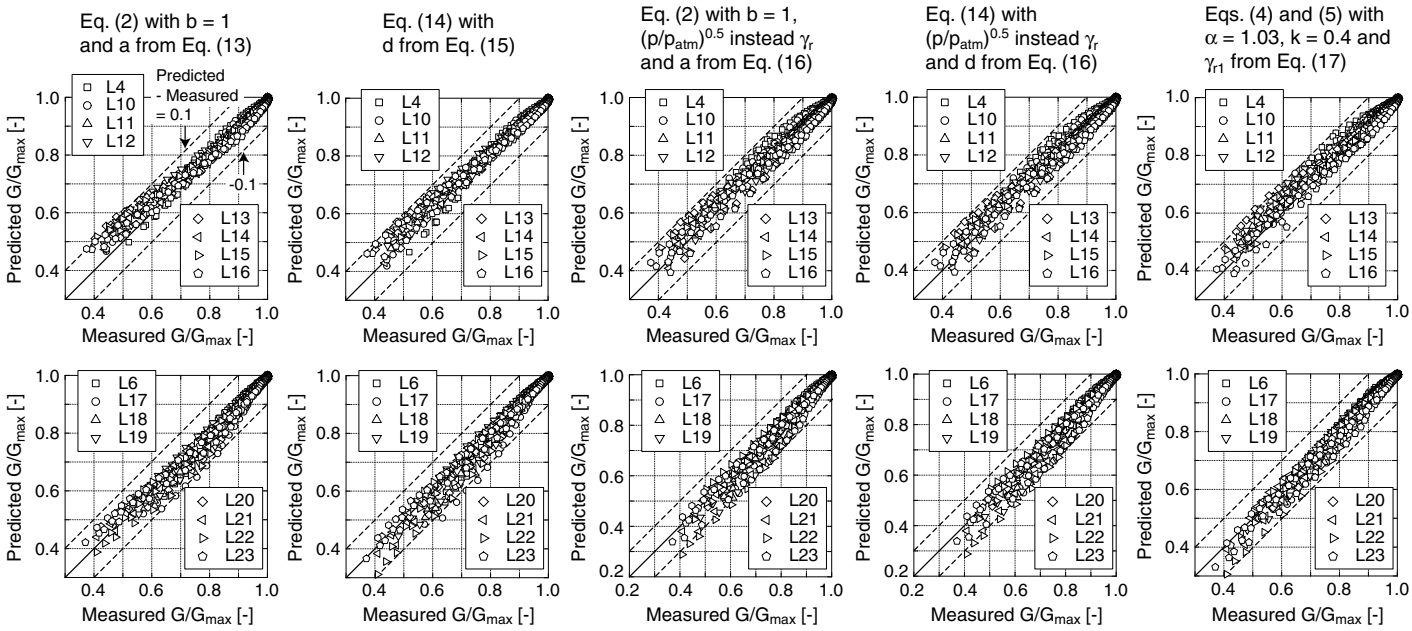

Fig. 5: *Predicted versus measured values of $G/G_{\max}$ for materials with d_{50} = 0.6 mm (upper row) or d_{50} = 2 mm (lower row) and various C_u-values. For each material the data from the four tests with different pressures and medium-dense specimens are shown.*

described by

$$\gamma_{r1}(D_{r0}) \quad = \quad 6.2 \cdot 10^{-4} \; [1 - 0.4(D_{r0} - 0.6)] \qquad (20)$$

The decrease of the exponent k of Eq. (5) with increasing uniformity coefficient can be approximated by:

$$k \quad = \quad 0.60 - 0.091 \; \ln(C_u) \qquad (21)$$

4.1.8 Summary of equations and correlations for $G/G_{\max}$

The C_u-dependent modulus degradation can be estimated from five different sets of equations:

1. Eq. (2) with $b = 1$ and a from Eq. (13)
2. Eq. (14) with d from Eq. (15)
3. Eq. (2) with $b = 1$, with $\sqrt{p/p_{\text{atm}}}$ instead of γ_r and with a from Eq. (16)
4. Eq. (14) with $\sqrt{p/p_{\text{atm}}}$ instead of γ_r and with $d = a$ from Eq. (16)
5. Eqs. (4) and (5) with $\alpha = 1.03$, $k = 0.4$ and γ_{r1} from Eq. (17)

The quality of prediction is inspected in Figure 5, where the predicted $G/G_{\max}$-values are plotted versus the measured ones. Most data points plot close to the bisecting line. Using the first set of equations in the list above, the differences between predicted and measured $G/G_{\max}$ data (analyzed for the experimental data with $G/G_{\max} < 0.9$) are less than 0.05 in 86% of cases, while they lie between 0.05 and 0.1 in 13% of cases. For the second, third, fourth and fifth sets of equations these values are 85/14%, 86/14%, 86/14% and 87/12%, respectively. Therefore, the prediction quality of the different sets of equations is quite similar. These observations are further inspected in Section 5.1 by means of literature data.

4.2 Damping ratio

Curves of damping ratio, D, versus shear strain amplitude, γ, are given exemplary for sand L20 in Figure 6. For a given shear strain amplitude, D decreases with increasing pressure while it is nearly independent of density. The data of the present study agrees well with the D-values reported by Kokusho [11] for Toyoura sand and similar pressures (gray shading in Figure 6). The data lie at the lower bound of the range of typical damping ratios reported by Seed et al. [25].

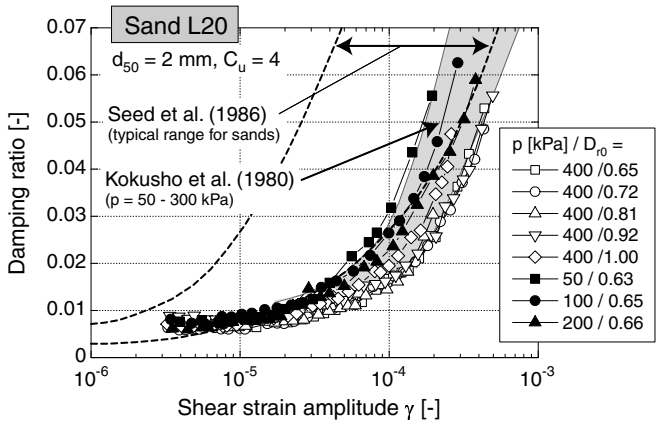

Fig. 6: *Damping ratio D versus shear strain amplitude γ for different mean pressures and relative densities*

4.2.1 Influence of d_{50} and C_u

The curves $D(\gamma)$ are not significantly affected by the mean grain size. This is evident in Figure 7a, where the curves $D(\gamma)$ of the sands and gravels L1 to L8 are compared. All curves were measured in tests on medium-dense samples at $p = 100$ kPa. A closer inspection of the d_{50}-influence is undertaken in Figure 7b,c, where the damping ratio, D, is plotted as a function of d_{50}. The data are provided for medium

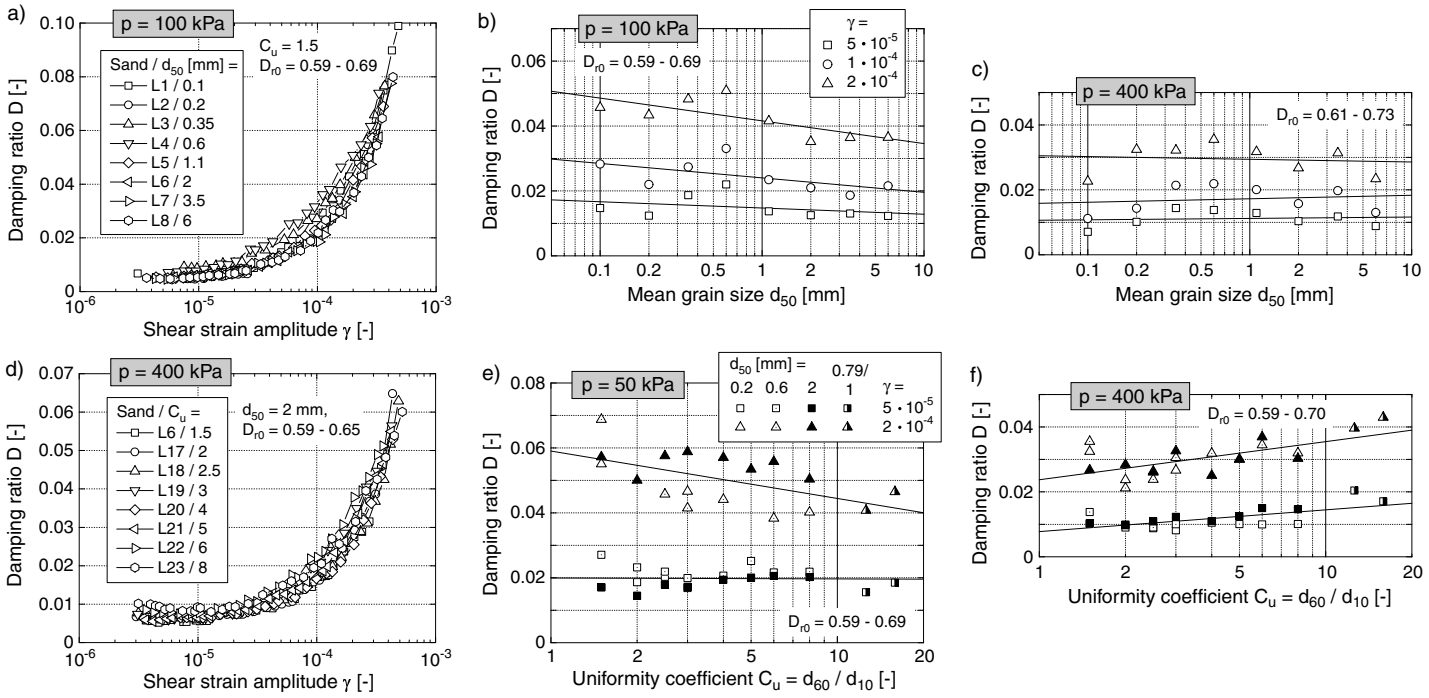

Fig. 7: *Dependence of damping ratio D on a)-c) mean grain size d_{50} and d)-f) uniformity coefficient C_u*

dense samples and for different pressures and shear strain amplitudes. For small pressures, D slightly decreases with d_{50} (Figure 7b) while it is nearly independent of d_{50} at larger pressures (Figure 7c). For practical purposes, this slight variation of D with d_{50} can be neglected in empirical formulas.

Figure 7d demonstrates that, in contrast to the modulus degradation curves, the curves $D(\gamma)$ are hardly influenced by the uniformity coefficient, C_u. The curves $D(\gamma)$ measured for materials with different C_u-values lie close to each other. The diagrams in Figure 7e,f allow a closer inspection and reveal that the C_u-influence on D is somewhat ambiguous. D is almost independent of C_u for small pressures and small shear strain amplitudes (Figure 7e). For small pressures in combination with larger shear strain amplitudes, D decreases with C_u (Figure 7e). An increase of D with increasing C_u was observed for large pressures, independent of the shear strain amplitude (Figure 7f). However, with reference to Figure 7d, it seems justified to neglect the C_u-influence in empirical equations for $D(\gamma)$.

4.2.2 Inspection of Hardin's equations (6) and (7)

If damping ratio, D, is plotted versus the normalized shear strain amplitude, γ/γ_r, with $\gamma_r = \tau_{max}/G_{max}$, the curves $D(\gamma/\gamma_r)$ for different pressures nearly coincide (Figure 8a). Eq. (6) overestimates the damping ratios measured in the present study (solid curve in Figure 8a), independently of the grain size distribution curve of the tested material. Figure 8b collects the curves $D(\gamma/\gamma_r)$ for most of the tested materials. These curves were measured at $p = 400$ kPa in tests on medium dense samples. Obviously, there is hardly any influence of the grain size distribution curve on the $D(\gamma/\gamma_r)$-data. The data in Figure 8b can be described by Eq. (7) with $b = 1$, modified by a minimum damping ratio, D_{min}, at small shear strain amplitudes:

$$\frac{D - D_{min}}{D_{max} - D_{min}} = \frac{\frac{\gamma}{\gamma_r}\left[1 + a\ \exp\left(-\frac{\gamma}{\gamma_r}\right)\right]}{1 + \frac{\gamma}{\gamma_r}\left[1 + a\ \exp\left(-\frac{\gamma}{\gamma_r}\right)\right]} \tag{22}$$

with $D_{min} = 0.006$, $D_{max} = 0.32$ and a = -0.64 (solid curve in Figure 8b). No significant influence of pressure and density on D_{min} could be found in the present study.

4.2.3 Normalization with $\sqrt{p/p_{atm}}$ instead of γ_r

The normalization of the shear strain amplitude with $\sqrt{p/p_{atm}}$ instead of γ_r works well also for the damping ratio. Figure 8c demonstrates that the curves $D(\gamma/\sqrt{p/p_{atm}})$ measured for the various granular materials fall into a narrow band, which can be approximated by Eq. (22) with $\sqrt{p/p_{atm}}$ instead of γ_r and with a constant $a = 843$ (solid curve in Figure 8c).

4.2.4 Correlation of $D - D_{min}$ with G/G_{max}

Figure 9 presents plots of $D - D_{min}$ versus G/G_{max}, exemplary for the materials L6, L21 and L23 having different C_u-values. Since the modulus degradation depends on the uniformity coefficient, the correlation between $D - D_{min}$ and G/G_{max} is also C_u-dependent. For each tested material, the data could be approximated by Eq. (8) (solid curves in Figure 9). In Figure 4h-i the parameters c_1 and c_2 of Eq. (8) are presented as functions of the uniformity coefficient. The decrease of c_1 and the increase of c_2 with C_u can be approximated by (solid lines in Figure 4h-i):

$$c_1 = 0.26 - 0.074\ \ln(C_u) \tag{23}$$

$$c_2 = -0.59 + 0.158\ \ln(C_u) \tag{24}$$

Eq. (8) with the parameters derived from Khouri [10] (dot-dashed curve in Figure 9) overestimates the data of the

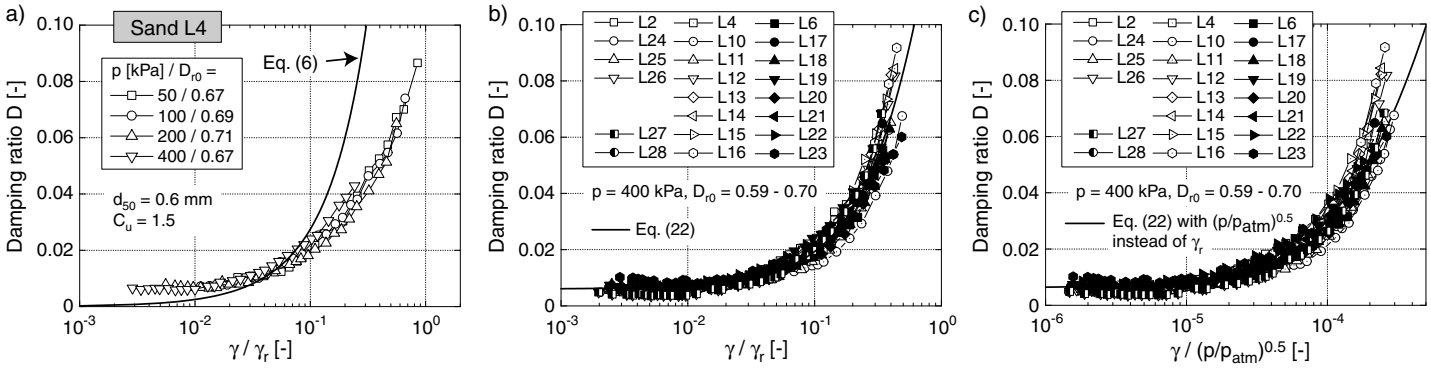

Fig. 8: *a) Damping ratio D as a function of γ/γ_r for sand L4; Comparison of curves b) $D(\gamma/\gamma_r)$ and c) $D(\gamma/\sqrt{p/p_{atm}})$ for different materials*

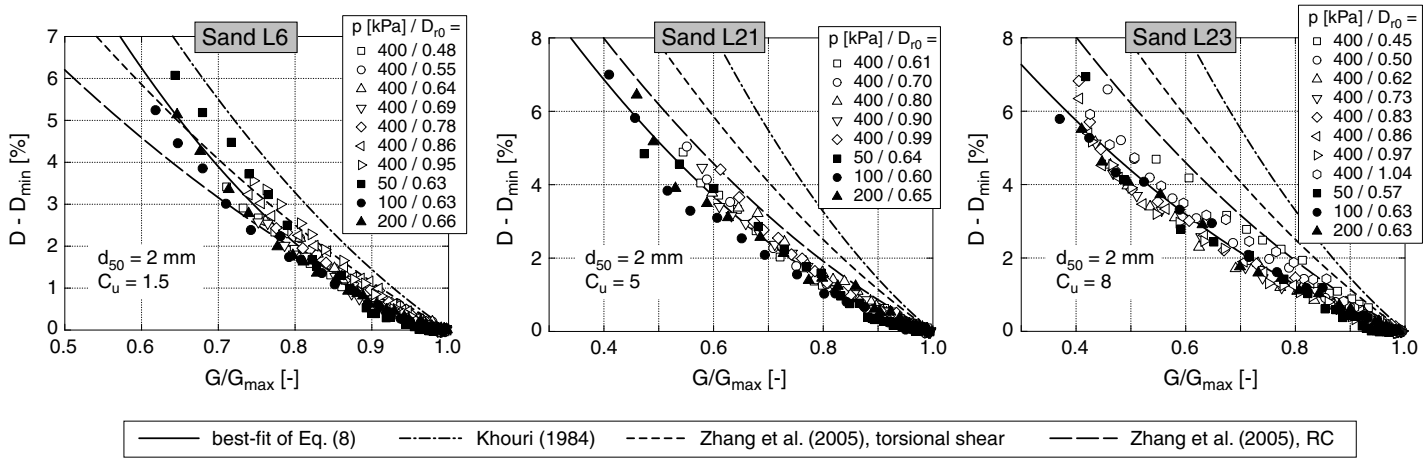

Fig. 9: *Damping ratio $D - D_{\min}$ as a function of $G/G_{\max}$*

present study, in particular for the well-graded materials. Eq. (8) with the constants proposed by Zhang et al. [40], either for torsional shear or RC test data (dashed curves in Figure 9), agrees well with the experimental data of the present study for intermediate uniformity coefficients $2 \leq C_u \leq 3$. However, the $D-D_{\min}$-values for poorly graded sands ($C_u = 1.5$) are slightly underestimated while the values for $C_u \geq 4$ are overestimated.

4.2.5 Summary of equations and correlations for D

The damping ratio can be estimated from three different sets of equations:

- Eq. (22) with $D_{\min} = 0.006$, $D_{\max} = 0.32$ and a = -0.64
- Eq. (22) with $\sqrt{p/p_{\text{atm}}}$ instead of γ_r and with $a = 843$
- Eq. (8) with Eqs. (23) and (24)

Using Eq. (22), the differences between predicted and measured damping ratio data (analyzed for the experimental data with $G/G_{\max} < 0.9$) are less than 0.01 in 80% of cases, while they lie between 0.01 and 0.02 in 14% of cases. For the second and third set of equations in the list above, these values are 83/15% and 93/6%, respectively. Therefore, the correlation between $D - D_{\min}$ and $G/G_{\max}$ delivers the best approximation of the measured D data. This is also confirmed by Figure 10 where the D values calculated from Eq. (8) are plotted versus the measured ones.

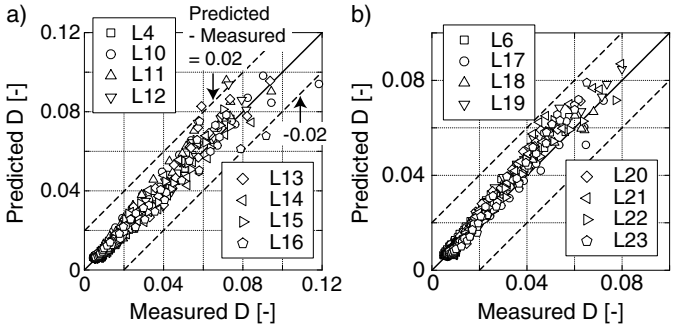

Fig. 10: *Damping ratios D predicted by Eq. (8) with Eqs. (23) and (24) versus measured D-values for materials with a) d_{50} = 0.6 mm and b) d_{50} = 2 mm and various C_u-values. For each material the data from the four tests with different pressures and medium-dense specimens are shown.*

4.3 Threshold amplitudes

The threshold shear strain amplitude indicating the transition from the linear elastic to the nonlinear elastic behaviour was defined as $\gamma_{tl} = \gamma(G/G_{\max} = 0.99)$ (Vucetic [31]). An increase of γ_{tl} with increasing mean pressure was observed (compare the curves $G(\gamma)/G_{\max}$ in Figure 2a-d). In Figure 11b-c, γ_{tl} is plotted versus d_{50} or C_u, respectively. The given γ_{tl}-values are mean values from the four tests with different pressures. A slight tendency for a decrease of γ_{tl} with in-

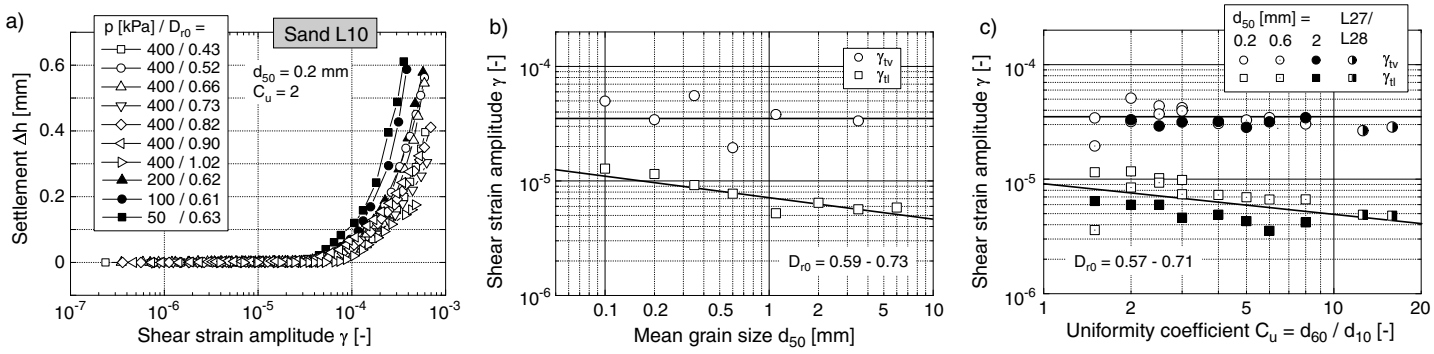

Fig. 11: *a) Settlement $\Delta h(\gamma)$ for different pressures and densities, shown exemplary for sand L10; Threshold shear strain amplitudes γ_{tl} and γ_{tv} in dependence of b) mean grain size d_{50} and c) uniformity coefficient C_u*

creasing values of d_{50} and C_u can be concluded from these diagrams. The mean values from all tested materials were $\gamma_{tl} = 4.2 \cdot 10^{-6}$, $6.1 \cdot 10^{-6}$, $8.2 \cdot 10^{-6}$ and $1.0 \cdot 10^{-5}$ for $p = 50$, 100, 200 and 400 kPa, respectively. These values lie slightly above the threshold amplitude $\gamma_{tl} \approx 3.0 \cdot 10^{-6}$ proposed by Vucetic [31] for granular materials.

Figure 11a shows typical curves of the settlement of the RC test specimens as a function of shear strain amplitude. In accordance with cyclic triaxial test data [34], the settlement increased with decreasing pressure, decreasing initial density and with increasing uniformity coefficient, C_u, of the tested material. The threshold shear strain amplitude at the onset of settlement, γ_{tv}, does not significantly depend on pressure and density. For each material mean values of γ_{tv} are plotted versus d_{50} or C_u, respectively, in Figure 11b-c. These diagrams demonstrate that γ_{tv} is almost independent of the grain size distribution curve. The mean value $\gamma_{tv} = 3.5 \cdot 10^{-5}$ obtained in the present study (upper solid line in Figure 11b-c) lies at the lower bound of the range $3 \cdot 10^{-5} \leq \gamma_{tv} \leq 4.0 \cdot 10^{-4}$ reported by Vucetic [31] for granular materials.

5 Comparison with data from the literature

5.1 Modulus degradation

Several $G(\gamma)/G_{\max}$ curves for clean sands were collected from the literature, together with the tested pressures and void ratios or relative densities. These $G(\gamma)/G_{\max}$ data are shown by the filled symbols or solid lines, respectively, in Figure 12a-u. Each diagram in Figure 12 belongs to a different sand or test series. In some studies (e.g. Ray & Woods [22], Yu [38]) the data are given in terms of a normalized shear strain γ/γ_r only. Such data are shown in the last three diagrams (v-x) in Figure 12. With the given values of p, e or D_r and C_u, the $G(\gamma)/G_{\max}$ data predicted by the five different sets of equations summarized in Section 4.1.8 have been calculated and compared with the experimental data. The prediction by Eqs. (4) and (5) with $\alpha = 1.03$, $k = 0.4$ and γ_{r1} from Eq. (17) is shown as dashed curves in Figure 12a-u. A good agreement between experimental and predicted data can be concluded for most of the data from the literature.

Slightly different curves $G(\gamma)/G_{\max}$ were reported in the literature for the same sand. For example (Figure 12a-d), for a given shear strain, the modulus degradation measured by Iwasaki et al. [8] (RC / torsional shear tests) and Lo Presti et al. [15] (RC) for Toyoura sand is larger than that reported by Kokusho [11] (undrained cyclic triaxial tests) and Wang & Tsui [33] (RC). This may be due to the different test devices, drainage conditions or batches of the tested sand. The prediction of the extended empirical equations derived from the present study is better for the data of Iwasaki et al. [8] and Lo Presti et al. [15] while the modulus degradation in the tests of Kokusho [11] and Wang & Tsui [33] is overestimated. For Monterey No. 0 sand (Figure 12e-g), the data of Iwasaki et al. [8] and Chung et al. [2] is predicted well, while the curves $G(\gamma)/G_{\max}$ measured for small pressures by Saxena & Reddy [23] cannot be reproduced. For Ottawa sand (Figure 12h-i), a good agreement of the prediction with the data of Shen et al. [26] and Hardin & Kalinski [7] (not shown in Figure 12) was found, while the modulus degradation observed by Alarcon-Guzman et al. [1] is slightly underestimated. The new correlations predict well the $G(\gamma)/G_{\max}$ curves measured for Ticino sand by Lo Presti et al. [16] (Figure 12j), for clean dry sand by Hardin & Drnevich [6] (Figure 12l), for several more well-graded sands by Iwasaki et al. [8] (Figure 12m-p), for Santa Monica beach sand by Lanzo et al. [12] (Figure 12q), for uniform HongKong beach sand by Li et al. [14] (Figure 12r) and for mortar sand tested by Menq & Stokoe [17]. The differences between measured and predicted data are larger for Leighton Buzzard sand tested by Li & Cai [13] (Figure 12k), "sand 2" studied by Wang & Tsui [33] (not shown in Figure 12) and parts of the crushed limestones studied by Hardin & Kalinski [7] (Figure 12s).

In contrast to the extended empirical equations for $G_{\max}$ discussed by Wichtmann & Triantafyllidis [35], there is no clear correlation between the quality of prediction and grain shape in Figure 12. For example, for Ottawa sand and Monterey No. 0 sand with subrounded to rounded grain shape, the modulus degradation is sometimes overestimated (Saxena & Reddy [23], Figure 12g), but in some other cases underestimated (Alarcon-Guzman et al. [1], Figure 12i).

Zhang et al. [40] proposed to apply Eqs. (4) and (5) with parameters α, k and γ_{r1} depending on the plasticity index PI and the geological age of the soil. The $G(\gamma)/G_{\max}$ curves of Zhang et al. [40] for PI = 0 and quaternary soil can be reproduced approximately with the author's equations for $C_u = 1.1$ (Figure 12t). The curves of Zhang et al. [40] for PI = 0 and tertiary or residual/saprolite soils are equivalent to the author's equations with $C_u = 4$ or 2.5, respectively. The $G(\gamma)/G_{\max}$ curve proposed for PI = 0 by Vucetic [31] can be reproduced well if the new correlations are applied with $C_u = 4$ (Figure 12u).

The prediction by the equations using $\sqrt{p/p_{\text{atm}}}$ as a reference quantity is similar to the dashed curves in Figure 12a-u. The prediction by the correlations necessitating an estima-

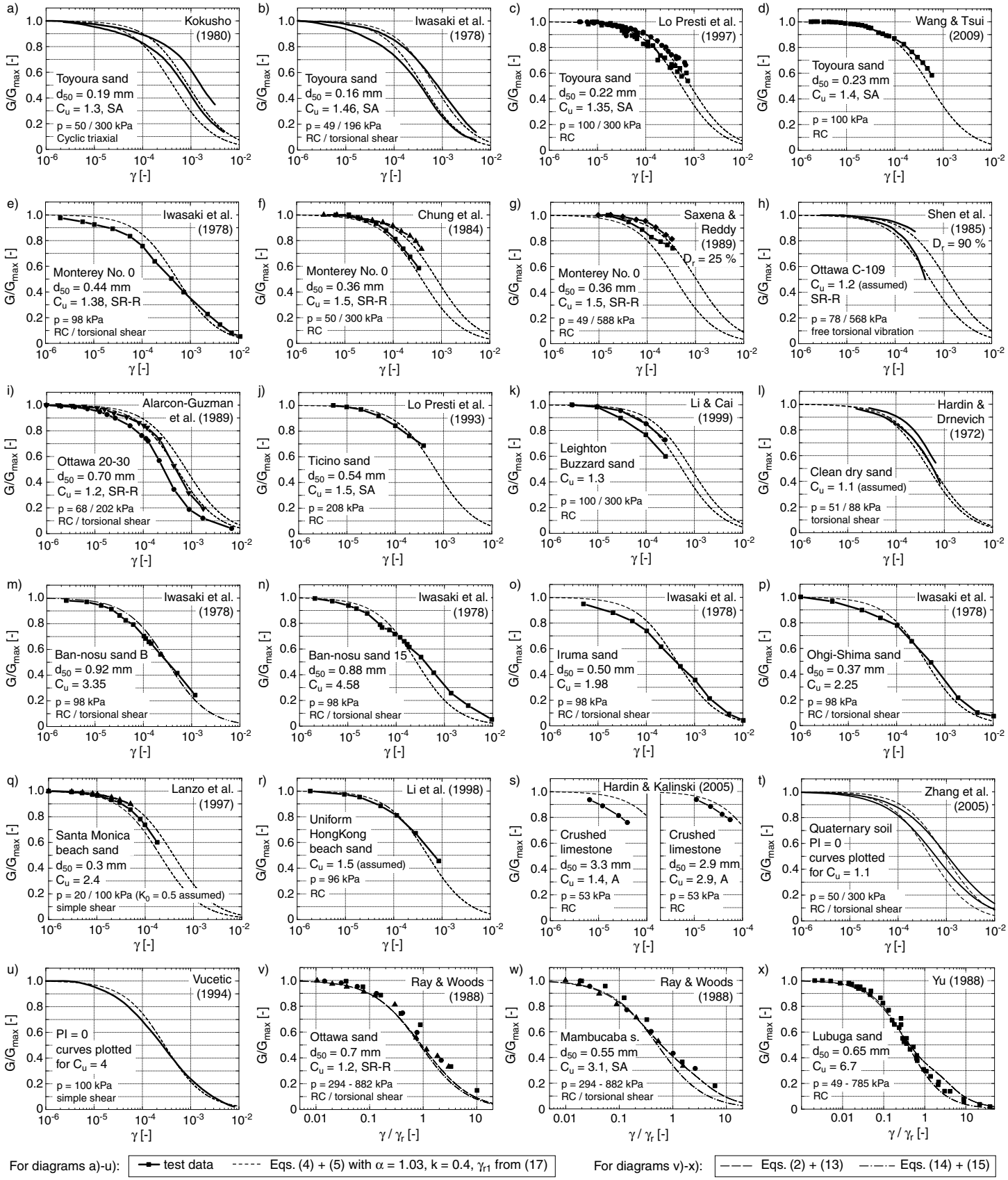

Fig. 12: *Comparison of $G(\gamma)/G_{\max}$ data for various sands from the literature with the prediction by the extended empirical equations (grain shape: R = round, SR = subrounded, SA = subangular, A = angular)*

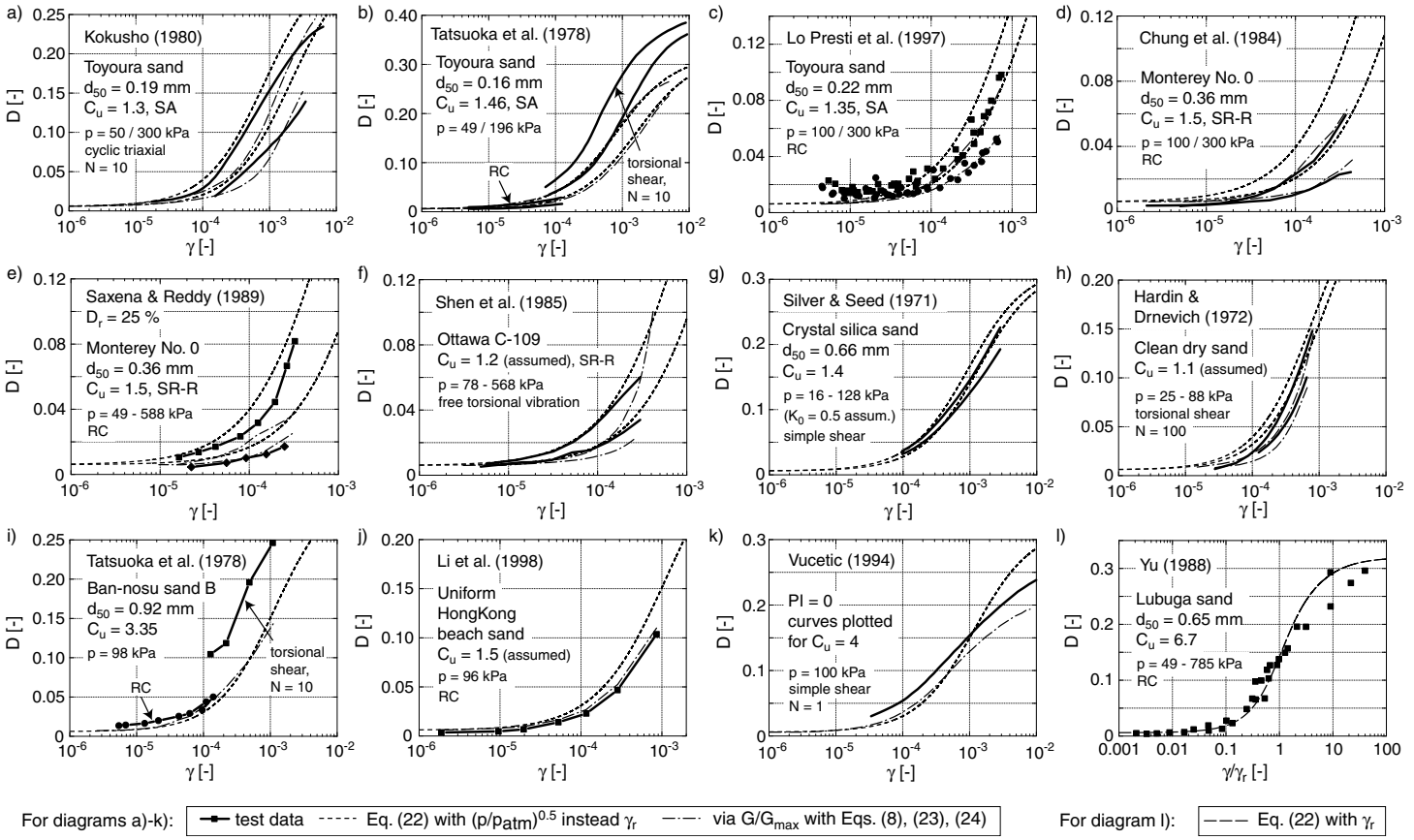

Fig. 13: *Comparison of $D(\gamma)$ data for various sands from the literature with the prediction by the extended empirical equations (grain shape: R = round, SR = subrounded, SA = subangular, A = angular)*

tion of the reference shear strain, γ_r, was found slightly more inaccurate, probably due to uncertainties in the γ_r-values calculated with estimations of $G_{\max}$ and $\tau_{\max}$.

The diagrams in Figure 12v-x demonstrate a good congruence between the $G(\gamma/\gamma_r)/G_{\max}$ data of Ray & Woods [22] and Yu [38] and the curves calculated from Eqs. (2) and (14) with the parameters from Eqs. (13) or (15), respectively. However, due to the uncertainties in the estimated γ_r-values, for practical purposes it is recommended to apply the extended Stokoe's equation (4) or the formulas using normalization with $\sqrt{p/p_{\mathrm{atm}}}$.

5.2 Damping ratio

A similar comparison with the literature has been undertaken for the damping ratio. Some of the curves $D(\gamma)$ collected from the literature are given as solid lines or filled symbols in Figure 13. The prediction by Eq. (22) with $\sqrt{p/p_{\mathrm{atm}}}$ instead of γ_r and with $a = 843$ has been added as dashed curves in Figure 13a-k. For some of the test series in the literature (e.g. RC test data for several sands measured by Tatsuoka et al. [30], Figure 13b,i, Shen et al. [26], Figure 13f, Silver & Seed [27], Figure 13g, Hardin & Drnevich [6], Figure 13h, Li et al. [14], Figure 13j), the prediction by Eq. (22) with $\sqrt{p/p_{\mathrm{atm}}}$ is satisfying, while in some other cases the experimental data are underestimated (torsional shear test data of Tatsuoka et al. [30], Figure 13b,i, simple shear tests of Vucetic et al. [32]) or overestimated (Chung et al. [2], Figure 13d, Saxena & Reddy [23], Figure 13e, Wang & Tsui [33], Khan et al. [9]). There is no clear tendency with grain shape or type of test. The differences could be due to equipment-generated damping (see Stokoe et al. [29], not determined in the present test series) or due to a different number of applied cycles, N. A significant decrease of D with N was found by several researchers (e.g. Hardin & Drnevich [5], Li & Cai [13]).

The curve $D(\gamma)$ proposed by Vucetic [31] for PI = 0 (Figure 13k) is approximately obtained with the same $C_u = 4$ that was necessary to reproduce the $G(\gamma)/G_{\max}$ data in Figure 12u. Similarly, the damping data of Zhang et al. [40] for PI = 0 is well reproduced with the same C_u-values applied for the shear modulus degradation.

Although the data $D(\gamma/\gamma_r)$ shown by Ray & Woods [22] and Yu [38] is well approximated by Eq. (22) with $D_{\min} = 0.006$, $D_{\max} = 0.32$ and $a = -0.64$ (Figure 13l), for most of the test series from the literature the prediction of Eq. (22) with γ_r as a reference quantity was found less reliable, probably due to an inaccurate estimation of the reference shear strain, γ_r.

If $G/G_{\max}$ measurements were available in the literature, these values were used to calculate the prediction of Eq. (8) with (23) and (24). As shown by the dot-dashed curves in Figure 12a-k, in most cases this prediction is closer to the experimental data than that of Eq. (22) with $\sqrt{p/p_{\mathrm{atm}}}$. Therefore, Eq. (8) with the correlations (23) and (24) is recommended for a practical application.

6 Micromechanical explanation for d_{50}-independence and C_u-influence

The d_{50}-independence of the curves $G(\gamma)/G_{\max}$ and $D(\gamma)$ observed in the experiments can be explained micromechanically by means of a simple cubic array of identical quartz spheres as described by Dobry et al. [3]. This theory, based on Mindlin [18] and Mindlin & Deresiewicz [19], predicts a shear modulus degradation with increasing shear strain amplitude according to

$$\frac{G}{G_{\max}} = \frac{2}{3}\frac{1-(1-\gamma/\gamma_t)^{3/2}}{\gamma/\gamma_t} \quad (25)$$

with the reference (threshold) shear strain, γ_t, being proportional to $\sigma^{2/3}$, where σ is the normal stress acting on the array of spheres. A similar equation giving D in terms of γ/γ_t has been also derived by Dobry et al. [3]. Since γ_t is independent of the diameter of the spheres, also the curves $G(\gamma)/G_{\max}$ and $D(\gamma)$ are independent of the grain size.

A micromechanical explanation for the larger modulus degradation in granular materials with higher uniformity coefficient can be given based on the study of force transmission chains in monodisperse and in polydisperse materials described by Radjai & Wolf [20] and Radjai et al. [21]. In a monodisperse material (particles of equal size) the force chains are rather equally distributed. In a polydisperse material (many different particle sizes), strong and weak force chains are formed through the interparticle contacts. With N_c denoting the contact normal force and N_c^{av} the average value of all contacts, the contact is defined as "strong" in case $N_c \geq N_c^{\text{av}}$ and "weak" if $N_c < N_c^{\text{av}}$. Numerical simulations of a polydisperse packing (Radjai & Wolf [20]) showed that the weak contacts transmit only approximately 28% of the average mean pressure in the granular packing. This means that a relatively small number of contacts in a polydisperse packing have large contact stresses and thus large reference shear strains, γ_t, while larger parts of the granular assembly have low γ_t values due to comparably low contact stresses. This may lead to a lower average γ_t value of the polydisperse packing compared to the monodisperse material. According to Eq. (25), for a given shear strain amplitude γ, lower γ_t-values mean a larger modulus degradation.

However, according to the theory of Dobry et al. [3], a decrease of γ_t with increasing C_u should be accompanied by an increase of damping ratio. This was not observed in the experiments. The damping mechanism in the theory of Dobry et al. [3] is based on sliding between loaded particles. In a polydisperse material, parts of the smaller grains with weak contacts will probably show a rolling contact behaviour, especially at larger shear strain amplitude, due to their lower γ_t-values. These small grains will act as a kind of lubricant for the larger grains. Rolling of grains involves a smaller dissipation of energy than the sliding mechanism, i.e., damping ratio decreases. These two mechanisms seem to compensate each other, leading to the C_u-independence of the curves $D(\gamma)$.

7 Summary, conclusions and outlook

The influence of the grain size distribution curve on the modulus degradation curves $G(\gamma)/G_{\max}$, on damping ratio $D(\gamma)$ and on the threshold shear strain amplitudes, γ_{tl} and γ_{tv}, was inspected based on the data from approximately 280 resonant column (RC) tests on 27 clean quartz sands with specially mixed grain size distribution curves. For each material, several RC tests with different relative densities and pressures were performed.

The test results show that the modulus degradation is not affected by the mean grain size, d_{50}, of the tested material. In contrast, for a certain shear strain amplitude, the ratio $G/G_{\max}$ significantly decreases with increasing uniformity coefficient, $C_u = d_{60}/d_{10}$. In order to consider this C_u-influence in common empirical equations for modulus degradation, the parameters of these equations have been correlated with C_u. The curves of damping ratio $D(\gamma)$ were found almost independent of the grain size distribution curve. However, the correlation between $D - D_{\min}$ and $G/G_{\max}$ is C_u-dependent. For a practical application, equations considering this C_u-influence have been developed. While the threshold shear strain amplitude γ_{tl} slightly decreases with increasing values of d_{50} and C_u, no significant influence of the grain size distribution curve on the threshold shear strain amplitude γ_{tv} could be found.

A good agreement between the prediction of the extended empirical equations and experimental $G(\gamma)/G_{\max}$ and $D(\gamma)$ data collected from the literature could be demonstrated. Furthermore, a micromechanical explanation of the observed dependencies has been provided.

In future work, the proposed correlations will be extended for sands containing fines and inspected for sands with gap-graded, stepwise linear, S-shaped or other naturally shaped grain size distribution curves.

Acknowledgements

The presented study has been performed within the framework of the project "Influence of the uniformity coefficient of the grain size distribution curve and of the fines content on the dynamic properties of non-cohesive soils" funded by the German Research Council (DFG, project No. TR218/11-1). The authors are grateful to DFG for the financial support. The RC tests have been performed during the former work of the authors at Ruhr-University Bochum, Germany.

References

[1] A. Alarcon-Guzman, J.L. Chameau, G.A. Leonardos, and J.D. Frost. Shear modulus and cyclic undrained behavior of sands. *Soils and Foundations*, 29(4):105–119, 1989.

[2] R.M. Chung, F.Y. Yokel, and V.P. Drnevich. Evaluation of dynamic properties of sands by resonant column testing. *Geotechnical Testing Journal, ASTM*, 7(2):60–69, 1984.

[3] R. Dobry, R.S. Ladd, F.Y. Yokel, R.M. Chung, and D. Powell. Prediction of pore pressure buildup and liquefaction of sands during earthquakes by the cyclic strain method. Technical Report 138, U.S. Department of Commerce, National bureau of standards, 1982. NBS Building science series.

[4] B.O. Hardin and W.L. Black. Sand stiffness under various triaxial stresses. *Journal of the Soil Mechanics and Foundations Division, ASCE*, 92(SM2):27–42, 1966.

[5] B.O. Hardin and V.P. Drnevich. Shear modulus and damping in soils: design equations and curves. *Journal of the Soil Mechanics and Foundations Division, ASCE*, 98(SM7):667–692, 1972.

[6] B.O. Hardin and V.P. Drnevich. Shear modulus and damping in soils: measurement and parameter effects. *Journal of the Soil Mechanics and Foundations Division, ASCE*, 98(SM6):603–624, 1972.

[7] B.O. Hardin and M.E. Kalinski. Estimating the shear modulus of gravelly soils. *Journal of Geotechnical and Geoenvironmental Engineering, ASCE*, 131(7):867–875, 2005.

[8] T. Iwasaki, F. Tatsuoka, and Y. Takagi. Shear moduli of sands under cyclic torsional shear loading. *Soils and Foundations*, 18(1):39–56, 1978.

[9] Z.H. Khan, G. Cascante, M.H. El Naggar, and C.G. Lai. Measurement of frequency-dependent dynamic properties of soils using the resonant-column device. *Journal of Geotechnical and Geoenvironmental Engineering, ASCE*, 134(9):1319–1326, 2008.

[10] N.Q. Khouri. Dynamic properties of soils. Master's thesis, Department of Civil Engineering, Syracuse, University, 1984.

[11] T. Kokusho. Cyclic triaxial test of dynamic soil properties for wide strain range. *Soils and Foundations*, 20(2):45–59, 1980.

[12] G. Lanzo, M. Vucetic, and M. Doroudian. Reduction of shear modulus at small strains in simple shear. *Journal of Geotechnical and Geoenvironmental Engineering, ASCE*, 123(11):1035–1042, 1997.

[13] X.S. Li and Z.Y. Cai. Effects of low-number previbration cycles on dynamic properties of dry sand. *Journal of Geotechnical and Geoenvironmental Engineering, ASCE*, 125(11):979–987, 1999.

[14] X.S. Li, W.L. Yang, C.K. Chen, and W.C. Wang. Energy-injecting virtual mass resonant column system. *Journal of Geotechnical and Geoenvironmental Engineering, ASCE*, 124(5):428–438, 1998.

[15] D.C.F. Lo Presti, M. Jamiolkowski, O. Pallara, A. Cavallaro, and Pedroni S. Shear modulus and damping of soils. *Géotechnique*, 47(3):603–617, 1997.

[16] D.C.F. Lo Presti, O. Pallara, R. Lancellotta, M. Armandi, and R. Maniscalco. Monotonic and cyclic loading behaviour of two sands at small strains. *Geotechnical Testing Journal, ASTM*, (4):409–424, 1993.

[17] F.-Y. Menq and K.H. Stokoe II. Linear dynamic properties of sandy and gravelly soils from large-scale resonant tests. In Di Benedetto et al., editor, *Deformation Characteristics of Geomaterials*, pages 63–71. Swets & Zeitlinger, Lisse, 2003.

[18] R.D. Mindlin. Compliance of elastic bodies in contact. *Journal of Applied Mechanics*, pages 259–268, 1949.

[19] R.D. Mindlin and H. Deresiewicz. Elastic spheres in contact under varying oblique forces. *Journal of Applied Mechanics*, 20:327–344, 1953.

[20] F. Radjai and D.E. Wolf. Features of static pressure in dense granular media. *Granular Matter*, (1):3–8, 1998.

[21] F. Radjai, D.E. Wolf, M. Jean, and J.-J. Moreau. Bimodal character of stress transmission in granular packings. *Physical Review Lett.*, 80(1):61–64, 1998.

[22] R.P. Ray and R.D. Woods. Modulus and damping due to uniform and variable cyclic loading. *Journal of Geotechnical Engineering, ASCE*, 114(8):861–876, 1988.

[23] S.K. Saxena and K.R. Reddy. Dynamic moduli and damping ratios for Monterey No. 0 sand by resonant column tests. *Soils and Foundations*, 29(2):37–51, 1989.

[24] H.B. Seed and I.M. Idriss. Soil moduli and damping factors for dynamic response analyses. Technical Report EERC 70-10, Earthquake Engineering Research Center, University of California, Berkeley, 1970.

[25] H.B. Seed, R.T. Wong, I.M. Idriss, and K. Tokimatsu. Moduli and damping factors for dynamic analyses of cohesionless soil. *Journal of Geotechnical Engineering, ASCE*, 112(11):1016–1032, 1986.

[26] C.K. Shen, X.S. Li, and Y.Z. Gu. Microcomputer based free torsional vibration test. *Journal of Geotechnical Engineering, ASCE*, 111(8):971–986, 1985.

[27] M.L. Silver and H.B. Seed. Deformation characteristics of sands under cyclic loading. *Journal of the Soil Mechanics and Foundations Division, ASCE*, 97(SM8):1081–1098, 1971.

[28] K.H. Stokoe, M.B. Darendeli, R.D. Andrus, and L.T. Brown. Dynamic soil properties: laboratory, field and correlation studies. In *Proc. 2nd Int. Conf. on Earthquake Geotech. Eng.*, volume 3, pages 811–845. A.A. Balkema, 1999.

[29] K.H. Stokoe II, S.K. Hwang, J. N.-K. Lee, and R. Andrus. Effects of various parameters on the stiffness and damping of soils at small to medium strains. Keynote lecture 2. In *IS Hokkaido 1994*, volume 2, pages 785–816, 1995.

[30] F. Tatsuoka, T. Iwasaki, and Y. Takagi. Hysteretic damping of sands under cyclic loading and its relation to shear modulus. *Soils and Foundations*, 18(2):25–40, 1978.

[31] M. Vucetic. Cyclic threshold shear strains in soils. *Journal of Geotechnical Engineering, ASCE*, 120(12):2208–2228, 1994.

[32] M. Vucetic, G. Lanzo, and M. Doroudian. Damping at small strains in cyclic simple shear test. *Journal of Geotechnical and Geoenvironmental Engineering, ASCE*, 124(7):585–594, 1998.

[33] Y.-H. Wang and K.-Y. Tsui. Experimental characterization of dynamic property changes in aged sands. *Journal of Geotechnical and Geoenvironmental Engineering, ASCE*, 135(2):259–270, 2009.

[34] T. Wichtmann, A. Niemunis, and T. Triantafyllidis. Validation and calibration of a high-cycle accumulation model based on cyclic triaxial tests on eight sands. *Soils and Foundations*, 49(5):711–728, 2009.

[35] T. Wichtmann and T. Triantafyllidis. On the influence of the grain size distribution curve of quartz sand on the small strain shear modulus $G_{\max}$. *Journal of Geotechnical and Geoenvironmental Engineering, ASCE*, 135(10):1404–1418, 2009.

[36] T. Wichtmann and T. Triantafyllidis. On the influence of the grain size distribution curve on P-wave velocity, constrained elastic modulus $M_{\max}$ and Poisson's ratio of quartz sands. *Soil Dynamics and Earthquake Engineering*, 30(8):757–766, 2010.

[37] T. Wichtmann and Th. Triantafyllidis. Influence of a cyclic and dynamic loading history on dynamic properties of dry sand, part II: cyclic axial preloading. *Soil Dynamics and Earthquake Engineering*, 24(11):789–803, 2004.

[38] P. Yu. Discussion of "Moduli and Damping Factors for Dynamic Analyses of Cohesionless Soils" by Seed et al. *Journal of Geotechnical Engineering, ASCE*, 114(8):954–957, 1988.

[39] P. Yu and F.E. Richart Jr. Stress ratio effects on shear modulus of dry sands. *Journal of Geotechnical Engineering, ASCE*, 110(3):331–345, 1984.

[40] J. Zhang, R.D. Andrus, and C.H. Juang. Normalized shear modulus and material damping ratio relationships. *Journal of Geotechnical and Geoenvironmental Engineering, ASCE*, 131(4):453–464, 2005.